This work was carried out in whole or in part within the framework of the NOMATEN Center of Excellence, supported from the European Union Horizon 2020 research and innovation programme (Grant Agreement No. 857470) and from the European Regional Development Fund via the Foundation for Polish Science International Research Agenda PLUS programme (Grant No. MAB PLUS/2018/8).

Journal of Nuclear Materials 568 (2022) 153848

Contents lists available at ScienceDirect

Journal of Nuclear Materials

journal homepage: www.elsevier.com/locate/jnucmat

Sputtering and reflection processes from amorphous lithium surfaces by low-energy impacts of H and D atoms and D_2 molecules

P.S. Krstic[a,b,*], E.T. Ostrowski[c], F.J. Domínguez-Gutierrez[d], S. Abe[c], B.E. Koel[c]

[a] Institute for Advanced Computational Science, Stony Brook University, Stony Brook, NY 11749, USA
[b] TheoretiK, Port Jefferson Station, NY 11776, USA
[c] Department of Chemical and Biological Engineering, Princeton University, Princeton, NJ, USA
[d] NOMATEN Centre of Excellence, National Centre for Nuclear Research, Andrzeja Sołtana7, 05-400 Otwock, Poland

ARTICLE INFO

Article history:
Received 20 March 2022
Revised 19 May 2022
Accepted 8 June 2022
Available online 9 June 2022

ABSTRACT

This work presents a computational study of the retention, reflection, and sputtering processes at amorphous and crystalline lithium surfaces by the impact of low energy (5-100 eV) hydrogen and deuterium atoms and D_2 molecules for a range of incident angles of 0° (normal to the surface) to 85°. Classical molecular dynamics simulations were performed with the reactive bond-order force field (ReaxFF) potentials. Effects of the temperature of the surface slab were also considered. The extent of retention, and the energy and angular distributions of reflected and sputtered atoms were determined. Comparison of the results of these simulations with available experimental data on the sputtering rate for Li atoms is in good agreement for incident angles of 0°, and the simulation results predict significant increase in the sputtering probabilities for incident angles larger than 30°.

1. Introduction

The plasma-material interactions (PMI) have a crucial role for the successful operation of a fusion reactor, strongly influencing the plasma performance and the material lifetime [1,2]. The plasma particles retained in the material significantly influence the fusion fuel recycling [3,4]. Lithium conditioning of plasma-facing components (PFCs) in the National Spherical Torus Experiment (NSTX) enhanced stored energy and plasma performance and suppressed edge localized modes (ELMs) [2], while complex chemistry controls both reflection of D and sputtering from the lithiated surfaces [3]. Understanding Li-based PMIs is of particular importance for the Lithium Tokamak Experiment (LTX-β), a low aspect ratio tokamak that operates in a low recycling regime enabled by Li-coated plasma facing surfaces [3,5]. At least 80% of the plasma-facing area of the LTX-β shells can be coated with Li, and heated to almost 650 K to provide a full liquid lithium plasma facing surface. While PMI with Li PFCs has been studied extensively in the past, much additional information is needed, especially for low-energy incident particles, to properly explain the relationship between Li PFCs and plasma performance and determine improved tokamak operating conditions [6–9]. This includes the study of chemical and physical erosion, reflection, sputtering, and H recycling of Li PFCs under these new conditions.

The subject of this paper is a study of the dynamics of Li surfaces when irradiated by H, D, or D_2 in the range of impact energies of 5-100 eV, where the computational data are scarce and inadequate, and the experimental data are not available. Probabilities of retention, reflection, and sputtering were calculated in the range of incident angles of 0° (normal to the surface) to 85°, to determine energy and angular spectra of ejected particles, and the effects of the surface structure (crystalline and amorphous) and surface temperature (300-600 K). For such a detailed study an atomistic approach is adequate, which takes care of specific covalent-ionic bond creation, breaking, and reconstruction present in interactions of hydrogen (H electronegativity of 2.2 [10,11]) with lithiated surfaces (Li electronegativity of 0.98). Quantum-classical molecular dynamics (QCMD) simulations based on the density functional tight binding (DFTB) method can correctly treat the change of the electron cloud during the classical dynamics of atoms, but this requires excessive computational time and resources [12–14]. While this is feasible for the study of hydrogen retention or chemical sputtering at low energies ($\leq$ 5 eV) [12,13], the study of these processes in a range of energies of 5-100 eV is computationally too intensive, not only because the calculation must be repeated for various energies, but also because higher energies require larger computational cells, i.e., a larger number of Li atoms in a target surface. For this reason, in this work, we chose to use classical molecular dynamics (CMD) based on a reactive bond-order

* Corresponding author at: Institute for Advanced Computational Science, Stony Brook University, Stony Brook, NY 11749, USA.
E-mail address: krsticps@gmail.com (P.S. Krstic).

https://doi.org/10.1016/j.jnucmat.2022.153848
0022-3115/

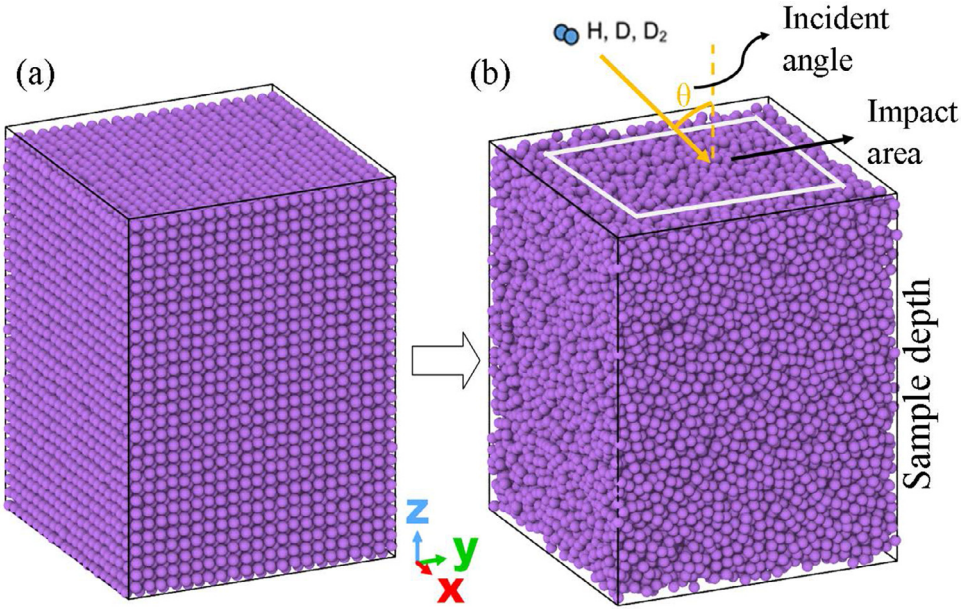

Fig. 1. Schematic of the particle-surface system for (a) crystalline, and (b) amorphous targets. Li atoms are depicted as purple spheres while H and D atoms are shown as blue spheres. Atoms in D_2 molecules were initially set at an internuclear distance of 0.7 Å (~ ground vibrational state), with randomly chosen directions of the internuclear axis.

force field (ReaxFF) [15,16], which showed in practice to be two orders of magnitude faster while still providing a similar accuracy [17,18] for the particle-surface processes to the QCMD with Sef-consistent charge DFTB [19] method. ReaxFF is implemented in the Large Scale Atomic/Molecular Massively Parallel Simulator (LAMMPS) code [16,20]. This approach was applied successfully in our previous work to study deuterium irradiation processes in lithium [21], and in boronized and lithiated carbon surfaces [12,13,22,23], and the results were benchmarked against QCMD calculations and available experimental data.

This paper is organized as follows. Section 2 provides a brief description of the computational approach used to prepare the target surface and obtain the results. Section 3 is the report on the calculated data. Section 4 contains the discussion and concluding remarks.

2. Computational method

All our computational results were obtained by CMD utilizing ReaxFF in LAMMPS. The Li surface target was a slab of either a monocrystalline BCC structure (lattice constant 3.609 Å) or an amorphous structure. The crystalline slab, after 3D energy minimization (adaptation to the ReaxFF), thermalization to 300 K, and relaxation to the surface boundary conditions and 2D periodicity, was occupying a box of dimensions 7.858 × 7.822 × 10.152 nm^3, containing 29,041 ^{7}Li atoms (Fig. 1a) with an average mass density of 0.536 g/cm^3, very close to the commonly reported Li solid density of 0.534 g/cm^3. Amorphization of the crystalline slab was done using the usual procedure, by repeated fast heating to 5000 K and slow annealing to 300 K with 3D periodicity, followed by relaxation to the surface boundary conditions and 2D periodicity (in the x- and y-directions). The final bounding box of the amorphous slab at 300 K was 8.00 × 8.00 × 10.22 nm^3, containing 28,704 Li atoms (Fig. 1b) with an average mass density of 0.506 g/cm^3, close to the known density of liquid lithium of 0.512 g/cm^3. The surface was treated as a NVE (microcanonical) ensemble by a Langevin thermostat with a time constant of 100 fs.

When a crystalline or amorphous cell is impinged upon by an atom of initial energy E_k and incident angle θ (Fig. 1b), the MD time step will depend on the impact energy. A time step that is too long might miss the interactions in the surface and tends to distort energy conservation. On the other hand, a time step that is too short would require a huge number of steps to describe the desired process. The optimal compromise of $\Delta t = 0.35$ fs for the MD time step in the impact energy range of 5-100 eV was found and applied for all calculations in this work. Trial calculations were done for 100 eV impact energy with steps in the range of 0.05-1 fs. The results for the probabilities of the processes started changing for steps larger than 0.35 fs, so this step was chosen. For lower energies, one could do similar experiments and obtain larger steps as sufficient, however keeping the same small time MD step for lower energies was a safe solution. All impact particles were launched in a vacuum from a height of 1 nm above the surface, where the particle-surface interaction is absent. It was found that $N = 1000$ repeated impacts at the surface for each initial parameter of the system (impact energy, incident angle, impact particle type, surface structure, temperature) and uniformly scanning the impact area of the surface (6 × 6 nm^2 in all cases, Fig. 1b) was sufficient to obtain a maximal statistical error (MSE) smaller than 20% in most of the calculated processes. The approximate MSE for all data was calculated as $p/\sqrt{n}$, where n is the sampled size of an outcome $p = n/N_S$, where N_S is the number of successful trajectories among the N impacts [24]. In many cases, the MSEs were within the size of the symbols used to graphically represent the data and might not be visible in the figures. Each impact was done independently on the identical surface, and only the position of impact of the particles at the surface was changing N times. These calculations qualify well for the so-called "embarrassing parallelization", where each computer node in a supercomputer is used for one trajectory. The reflection, retention, and sputtering probabilities were always obtained "on the same footing."

The Lindemann index δ, as used herein, and as defined and utilized in ref. [25], was used to measure the thermally driven disorder in our clusters. It is calculated as follows:

$$\delta = \frac{2}{M(M-1)} \sum_{i<j} \frac{\sqrt{\langle r_{ij}^2 \rangle - \langle r_{ij} \rangle^2}}{\langle r_{ij} \rangle} \quad (1)$$

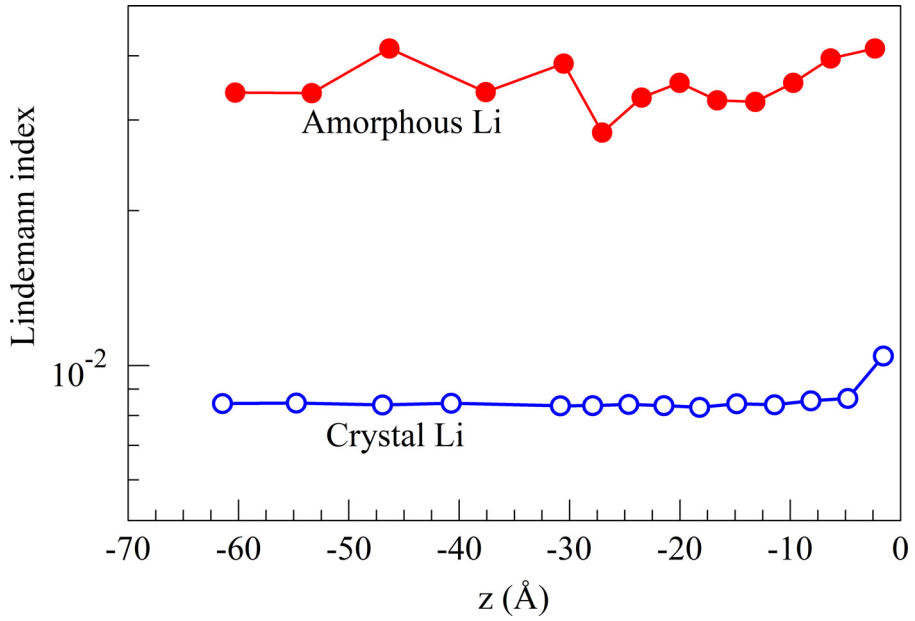

Fig. 2. Values of the Lindemann index for slices of 1000 atoms into the bulk from the top surface in both crystalline and amorphous Li at 300 K.

where r_{ij} is the distance between the i-th and j-th atom, M is the number of atoms in the system, and the average was calculated over 1 ps. The distribution of the Lindemann index over the surface depth was calculated in slices of 1000 atoms, and the results for both crystalline and amorphous Li surfaces are shown in Fig. 2 for 300 K and up to the depth of about 6 nm. The Lindemann index is constant along the depth of the crystalline sample, with some disorder at the top slice facing vacuum.

There is less uniformity present along the depth of the amorphous Li surface, which also shows increased disorder toward the top surface of the slab. The Lindemann index values for the amorphous slab show a good degree of amorphization, being about four times larger than those for near the crystalline surface.

It is useful to see how well a sample surface is thermally equilibrated at desired temperatures, i.e., thermalized by a Langevin thermostat, relaxed with the surface boundary conditions, and prepared for irradiation by hydrogen atoms. A comparison of the Li atom kinetic energy distribution in an amorphous Li surface thermalized to 300 K with fits to Maxwellian distributions at 364 K (the best fit) and 300 K is shown in Fig. 3. The points for the Li distribution were obtained from averaging counts in 15 bins of 700 data points. The differences in the width of the distributions and position of the peaks for the Li sample and Maxwellian distributions at 300 K are a result of the finite number of particles in the Li sample, the quality of the Langevin thermostat and, the binning procedure in obtaining the curve for the Li sample.

3. Results and discussion

3.1. Reflection

As discussed in Section 2, the probabilities of reflection P_R are calculated for each impact energy and angle as a ratio of the number of reflected trajectories (N_R) and the total number of successful trajectories N_S, with P_R=N_R/N_S. The number of successful trajectories Ns is often smaller than the number of applied projectiles, usually because of a computer glitch or different computer times at various nodes in the "embarrassing parallelization" mode we apply. Most of the incident D_2 molecules were dissociated upon impact with the surface, leading to several cases: 1) both incident atoms reflected, 2) one incident atom reflected and one was retained in the surface, and 3) both incident atoms were retained in the slab. Probabilities of reflection in the D_2 case were obtained by counting the reflected D atoms, and therefore the probability of reflection per D atom impact. The probabilities of retention per D impact, P_{ret}, are in all cases defined by particle conservation, i.e., P_{ret}=1-P_R.

As seen in Fig. 4a, the values of P_R for H incident on amorphous Li are much weaker functions of impact energy (E) than of the angle of incidence (θ), especially for small values of θ. Thus, when θ changes from 0° (normal to the surface) to 85°, P_R increases about two times for E = 5 eV and four times for E = 100 eV. However, when E changes from 5 eV to 100 eV, P_R shows almost no change with incident angle for $\theta \leq 30°$, but then increases almost three times for θ = 85°. For impact perpendicular to the surface (θ = 0°), P_R for H has a weak variation with impact energy in the range of E = 10-100 eV, with a maximum at E = 25 eV. This localized maximum is not visible for larger incident angles. When θ = 0°, the weak decrease of P_R with E, for E > 50 eV, can be ascribed to the deeper penetration of the particles upon impact, which makes retention in the surface more probable. This trend was also seen in VFTRIM calculations for D impacts [26]. P_R for D impact at θ = 0° is about two times smaller than that for H impact. This is a consequence of the mass difference between D and H, which leads to a more efficient transfer of kinetic energy to the Li atoms by D than by H. Consequently, incident D atoms have a shallower penetration depth as shown later in this section and in Section 3.3 and will also lose more energy in the collision cascade on the way out of the surface. Finally, the reflection probability of incident D from a monocrystalline Li surface overlaps with that of incident D from an amorphous Li surface for θ = 0° and $E \leq$ 10 eV but decreases rapidly with increasing impact energy. The incident angle for calculations using the crystalline surface was set to 5° rather than 0° to mitigate channeling effects at higher energies.

It is interesting that for perpendicular impacts of incident D_2, the reflection probability P_R (per D) is only slightly smaller than that of incident D when $E \geq$ 25 eV, but this difference greatly increases toward lower energies. This is a known consequence [24] of the fact that most of the incident D_2 particles use a fraction of their energy (~4.5 eV) to dissociate before they reflect. If the P_R curve for incident D_2 is shifted by 4.5 eV toward lower energies, the D_2 reflection curve stays only slightly lower than the D curve

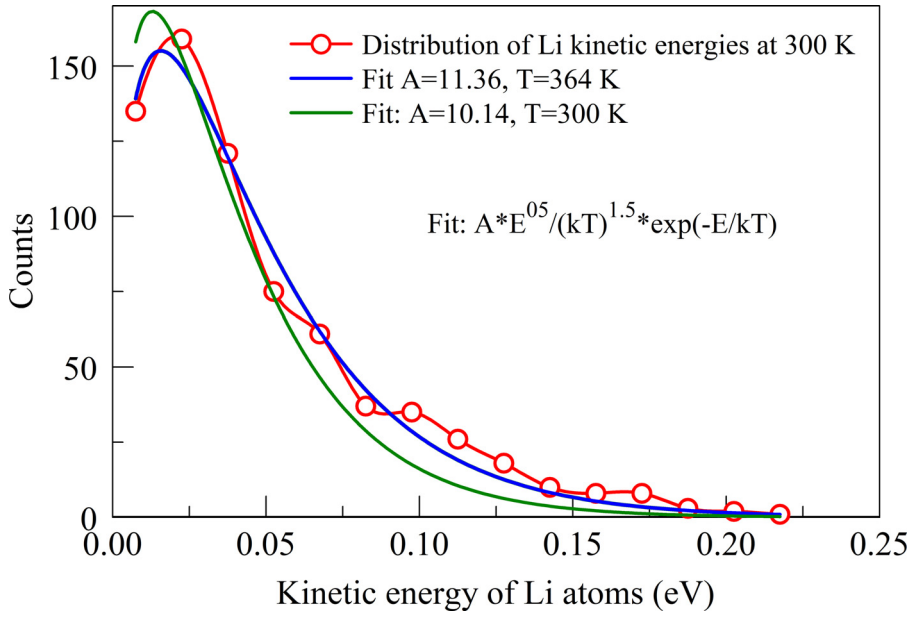

Fig. 3. Comparison of the distribution of the Li atom kinetic energies with Maxwellian energy distributions at $T = 364$ K (best fit) and $T = 300$ K.

over the entire energy range. The P_R curve for D_2 impacts is lower than the one for D impacts because more D atoms from dissociated D_2 are retained than reflected, and this difference decreases with increasing impact energy. As seen in Fig. 4b, the P_R values for $\theta = 45°$ are about a factor of two higher than for $\theta = 0°$.

Fig. 4a indicates that the retention probability P_{ret}=1-P_R of incident H is small at almost grazing angles of incidence (85°) for the considered energy range, falling to about 20% at $E = 100$ eV. At normal incidence ($\theta = 0°$) P_{ret} of D is close to 90% in the considered energy range, significantly larger than P_{ret} of H (around 80%). The value of P_{ret} for incident D in crystalline Li is 88% at $E = 10$ eV but increases to over 95% for $E = 100$ eV.

The dependence of the reflection probability P_R on the angle of incidence θ for H impact on an amorphous Li surface at 300 K is plotted in Fig. 5 for several impact energies. Notably, there is not a strong dependence of P_R on the impact energy at $E \geq 50$ eV. The data points for the 50, 75, and 100 eV trajectories can be fit by a power function of the angle of incidence θ according to

$$P_R(\theta) = A\theta^b + C \tag{1}$$

with $A = 1.274 \times 10^{-5}$, $b = 2.38$, and $C = 0.264$, where θ is in degrees. If extrapolated to grazing incidence ($\theta = 90°$), the fit gives $P_R(90°) \sim 0.82$, i.e., P_{ret} of H is minimally 18% in the considered range of impact energies.

An analysis of the energies and angles of the reflected H atoms is conducted. The average of the reflected atoms kinetic energies (E_R) over all reflected trajectories (n_R) for each impact energy and angle is calculated as $E_{av} = E_R/n_R$. Interestingly, the ratios of E_{av} to the impact atom energies (E), E_{av}/E, are slowly varying functions of E, but strong functions of the incident angle θ (Fig. 6). Thus, for $\theta \leq 30°$ this ratio is between 0.4 and 0.48 for 5 eV $\leq E \leq$ 100 eV. However, for $\theta = 85°$, E_{av}/E increases substantially and is in the range of 0.55 to 0.83. Significantly lower values of E_{av}/E are observed for the reflected D atoms from the crystalline Li surface. For an incident angle of 5°, the E_{av}/E values vary between 0.25 and 0.3, like the values reported by Qui and Ruzic [27], obtained by MD and TRIM-SP.

The weak dependence of $P_R(E)$ enables the possibility of averaging values of E_{av}/E over the impact energy E for each angle of incidence θ, as is done in Fig. 7. These average values $[E_{av}/E]_E$ can be fitted to a power function of θ, i.e., $[E_{av}/E]_E(\theta) = S\theta^r + Q$, where $S = 2.72 \times 10^{-5}$, $r = 2.0845$, $Q = 0.4457$, and θ is in degrees. Thus, at perpendicular incidence $\theta = 0°$ the energy of reflected H atoms is about 45% of the impact energy, while for grazing incidence the energy of reflected H atoms is about 75% of the impact energy. The total variations of E_{av}/E around the average value are shown in Fig. 7 as min-max margins.

The angular distributions of H atoms reflected from the Li surface, $dN/d\Omega$, are calculated from [29–31]

$$\frac{dN}{d\Omega} = C\frac{N(\theta, \delta\theta)}{2\pi\,\delta\theta\,\sin\theta} \tag{2}$$

where $N(\theta, \delta\theta)$ is the number of reflected particles into interval $\delta\theta$ centered at θ, and C is a normalization constant. The distributions $dN/d\Omega$ for reflected H atoms, with an impact energy of 100 eV, from an amorphous Li surface, normalized to each incident angle (shown by arrows), are presented in Fig. 8.

While all the distributions show similar diffuse features at small angles, a pronounced specular peak is visible for data using an 85° angle of incidence. This is consistent with the trend of an increase of the average reflection velocity with angle of incidence even when averaged over impact velocities, which suggests further increase of the reflection velocity, eventually reaching the impact velocity at the grazing angle of incidence.

The features of the angular distributions of reflected H from crystalline Li are different than those from amorphous Li surfaces, as shown in Fig. 9 for a 5° angle of incidence at several impact energies. Due to the Li crystalline structure, the reflected H angular distributions show some oscillatory features, with a pronounced specular peak at the lowest reflection angles.

As a measure of the quality of the calculated results with respect to the surface slab size, cumulative, normalized distributions from over 1000 trajectories of the maximum penetration depth were calculated only from those impact atoms (H and D) that were reflected. These penetration depths are referred to herein as the “depths of reflection” and their distributions are shown in Fig. 10 for various impact energies and incident angles. The “reflection depth limits”, shown as thin horizontal lines, indicate the regions where 95% of the incident H atoms undergo reflection. This depth limit is crossed at about 8 nm for perpendicular H impacts at 100 eV for amorphous Li at 300 K (Fig. 10a), but at 1.5

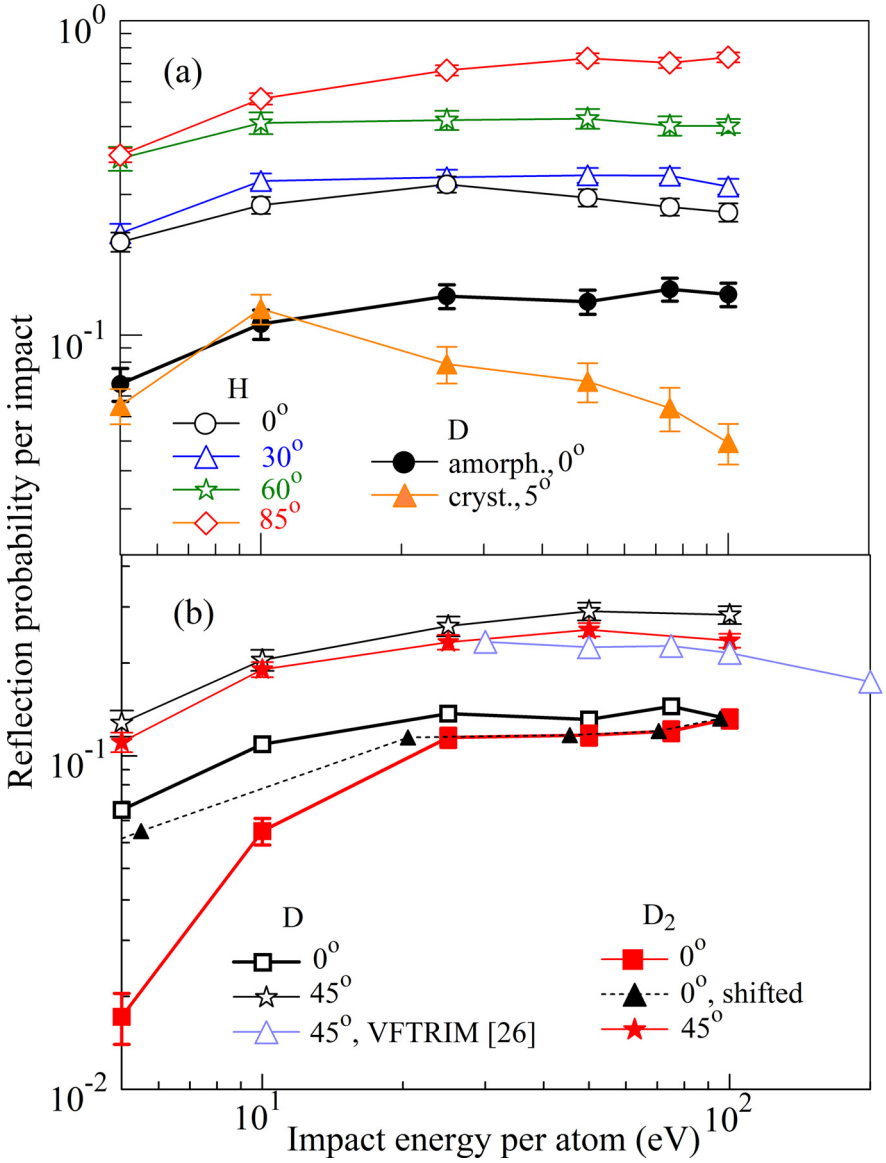

Fig. 4. Probabilities of reflection per impact P_R of (a) H and D, and (b) D_2 and D, impinging on an amorphous Li surface at 300 K for a range of impact energies of 5-100 eV, for various angles of incidence of 0-85°. D impacts at a crystalline Li surface at 5° incidence are shown for comparison. Each point is an average from about 1000 trajectories. Error bars shown are for maximal standard errors.

nm for perpendicular H impacts at 10 eV. At an incident angle of 85° (Fig. 10c), 95% of 100-eV H atoms are reflected at depths less than 4 nm, while for 10-eV impacts that depth is only about 0.5 nm. Compared to H atoms, D atoms at perpendicular incidence (Fig. 10b) have a smaller depth limit than H atoms in the amorphous Li surface, which is 6 nm for 100-eV perpendicular impacts and 1 nm for 10-eV impacts. Finally, D impact at a Li crystalline surface (Fig. 10d) at a 5° angle of incidence further reduces the limiting depth of reflection, which is now 4.5 nm for 100-eV and 0.4 nm for 10-eV incident energies.

3.2. Sputtering

The sputtering yield per impact atom is calculated for each impact energy and angle of incidence as a ratio of the number of sputtered Li trajectories n_{sp}, and the total number of successful trajectories N_S, i.e., $P_{sp}=n_{sp}/N_S$. Li is sputtered mainly in the form of Li atoms. When sputtered Li appears in the form of molecules (Li_2) or small Li clusters (more than two atoms), the sputtering probability is calculated by counting all ejected Li atoms.

As shown in Fig. 11, the values of P_{sp} for incident H at an amorphous Li surface are strong functions of the impact energy E, especially for $E \leq 50$ eV, and this is true for all angles of incidence. Thus, when E changes from 5 to 50 eV, P_{sp} increases by more than an order of magnitude when $\theta = 0°$ and more than two orders of magnitude when $\theta = 85°$. For H impacts at $\theta = 0°$, P_{sp} shows even a small drop of 10% when the energy increases from 50 eV to 100 eV. For larger angles of incidence, this small drop is not observed. For $\theta = 30°$, P_{sp} increases by 10% over the same interval of E, and this rate of change is present for all larger incident angles. Our calculations of sputtering yields by perpendicular D impacts at an amorphous Li surface show a slight increase in P_{sp} as the impact energy increases from 50 to 100 eV, unlike the trend of H over the same energy range. However, there is an apparent saturation of the sputtering yield from a Li crystalline surface with increasing D impact energy, and somewhat smaller sputtering yields than from amorphous Li surfaces. The TRIM calculations of Majeski et al. [3] significantly underestimate P_{sp} for $E < 100$ eV as expected, since TRIM only describes physical sputtering, which is the dominant sputtering mechanism at high impact energies

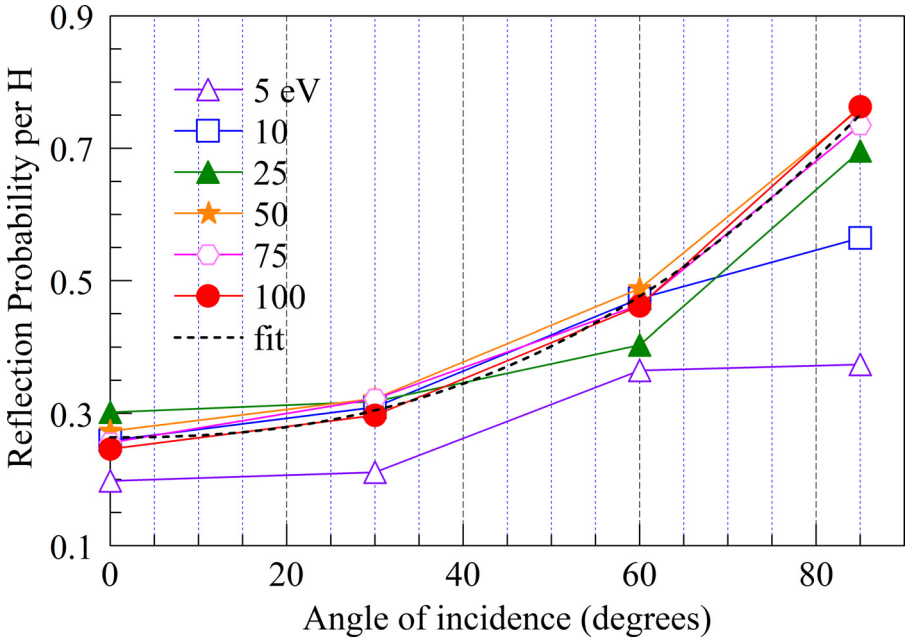

Fig. 5. Probability of reflection P_R for various impact energies of H as function of angle of incidence on an amorphous Li surface at 300 K. Fitted curves are explained in the text. The probabilities are an average over 1000 trajectories.

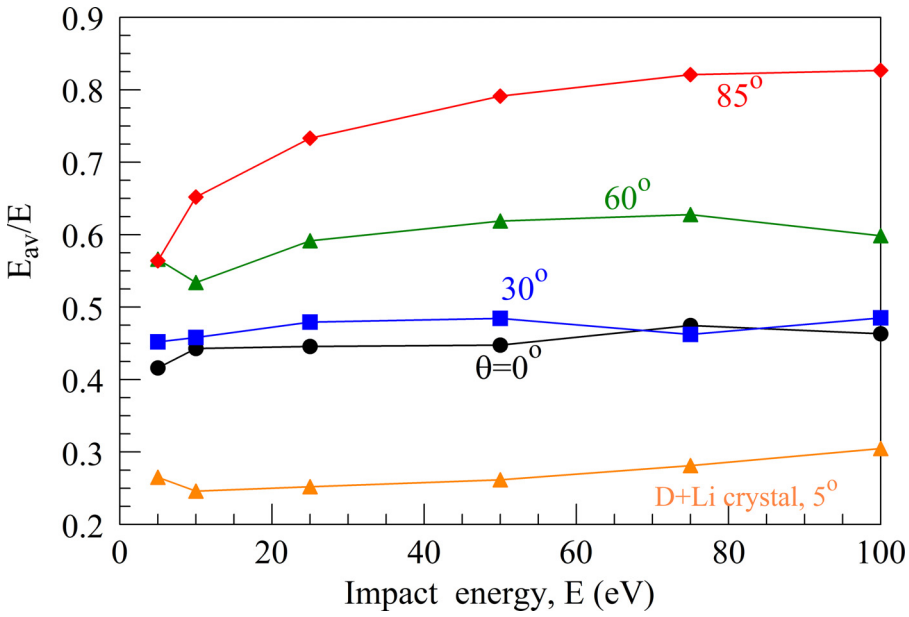

Fig. 6. Energies of the reflected atoms (E_{av}) from an amorphous Li surface at 300 K, averaged over 1000 trajectories, and normalized to the impact energy (E) of the incident particle for various angles of incidence. The incident atoms are H unless otherwise labeled.

(> 100 eV). Below 100 eV, however, chemical sputtering is the dominant mechanism, which will be explained in more detail later in this subsection.

Average sputtering probabilities per D atom from an amorphous Li surface at 300 K by impact of D_2 molecules having incident energies in the range of 5-100 eV and at incident angles of $\theta = 0°$ and $\theta = 45°$ are shown in Fig. 12. For comparison, calculated values of P_{sp} by incident D atoms are also shown. The dependence of the sputtering probability on the impact energy E is almost identical for D atoms and D_2 molecules when the impact energy of D_2 is represented on a per atom basis. Our calculated results for the D sputtering probabilities at $E = 100$ eV tend to agree with the experimental results for $E > 100$ eV [9,25], which are shown for comparison in Fig. 12.

The explicit dependence of the sputtering yield per H atom on the angle of incidence of H atom impacts at the amorphous Li surface is shown in Fig. 13 for various impact energies. In all cases, the sputtering yield per H increases for increasing incident angle. While for 5 eV and 10 eV impact energies the $P_{sp}(\theta)$ is a weak function of θ, Fig. 13 shows for $E \geq 25$ eV that P_{sp} increases by a factor of about four when θ changes from 0° to 85°. $P_{sp}(\theta)$ for $E \geq 50$ eV can be fitted to a power function $P_S = U\theta^w + V$, where $U = 6.131 \times 10^{-4}$, $w = 1.208$, $V = 0.055$, and θ is in degrees. The resulting fit is plotted as the dashed line in Fig. 13.

Average kinetic energies E_{sp} of the sputtered Li atoms, obtained by averaging over 1000 trajectories for each impact energy E of incident H atoms and each angle of incidence, are plotted in Fig. 14 as a function of the H impact energy. Li atoms are the domi-

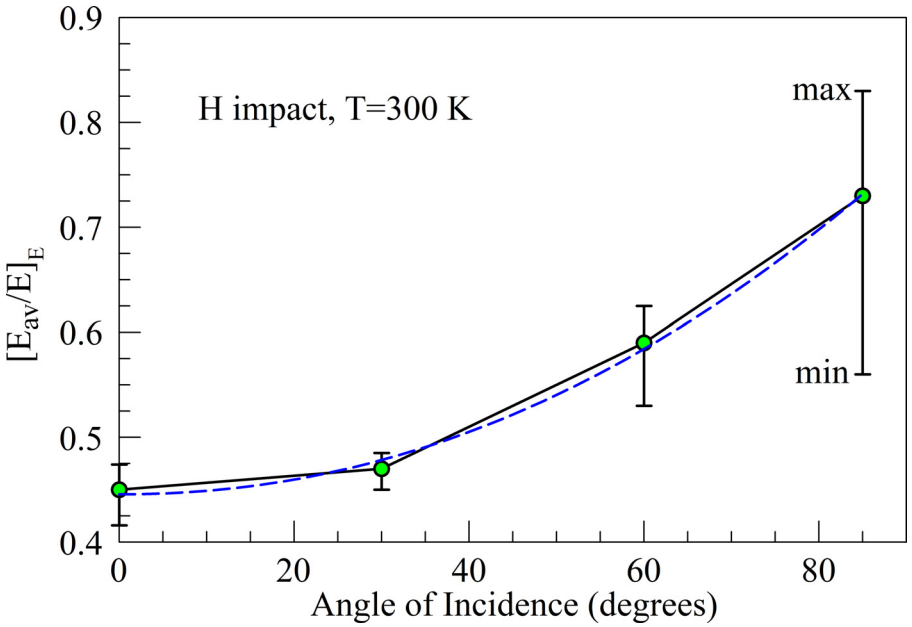

Fig. 7. Energies of reflected H atoms, normalized by their impact energy and averaged over both trajectories and impact energies $[E_{av}/E]_E$ (solid line). The fitted curve (dashed line) is explained in the text.

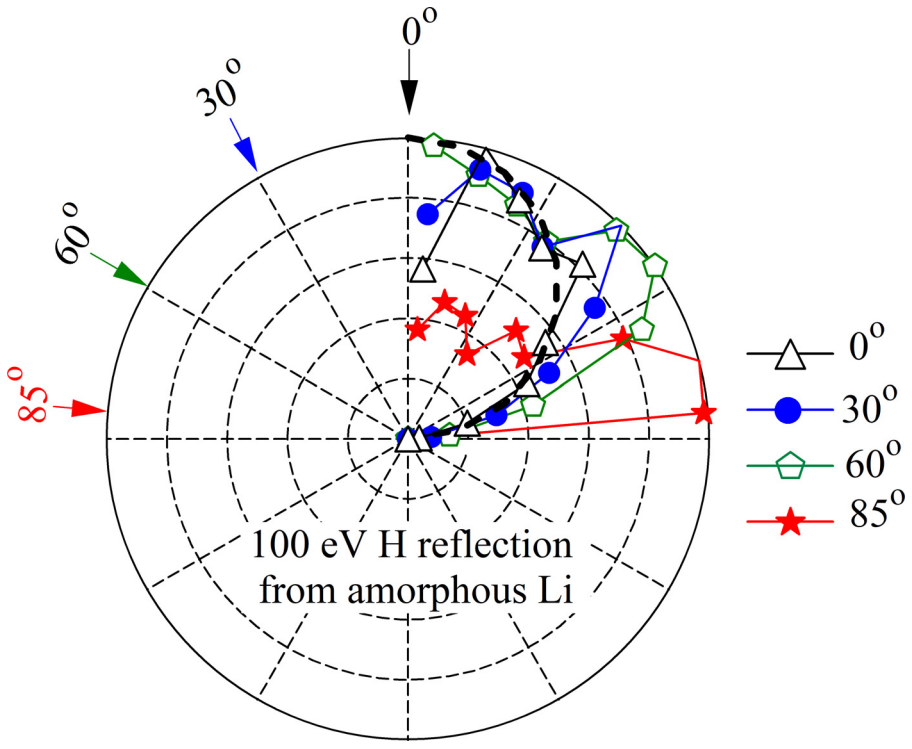

Fig. 8. Angular distributions of H, with an impact energy of 100 eV, reflected from an amorphous Li surface at 300 K for various angles of incidence. The distributions are shown in the form of polar diagram with the reflected particle curves normalized to unity at their maximum values. The Lambert cosine law is shown by a dashed line for reference.

nant sputtered species, with much fewer Li_2 and no LiH detected as sputtered species in 1000 trajectories, for all E. Interestingly, all cases shown in Fig. 14 (except for near grazing incidence at $\theta = 85°$) follow a similar trend with respect to impact energy, almost independent of the angle of incidence. The dashed curve in Fig. 14 shows the arithmetic average of $E_{sp}(E)$ for $\theta \leq 60°$.

Two curves are also shown for $E_{sp}(E)$ for D impact at amorphous and crystalline Li surfaces and these are similar to those for H impact at the amorphous Li surface. The energy of the sputtered Li atoms increases with impact energy when $\theta \leq 60°$, at an average value of about 0.1 eV for each 10-eV increase in impact energy to an E_{sp} value of 0.8-1 eV for a 100 eV impact energy. The influence of the impact energy on the sputtered energies is larger for $\theta = 85°$, and E_{sp} reaches 1.2 eV at $E = 100$ eV.

The trends seen in Fig. 14 for the kinetic energies of sputtered Li atoms indicate a possibility to average E_{sp} over the range of incident energies to determine a new value $E_{a,sp}$, which is plotted in Fig. 15, as well as the min-max values of E_{sp}, for several incident

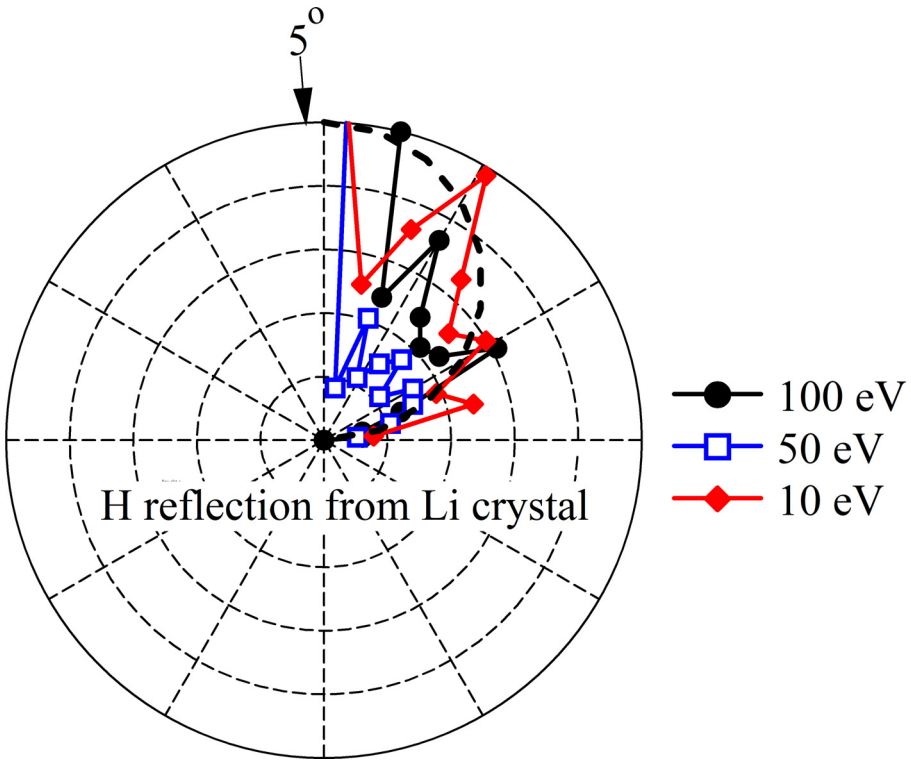

Fig. 9. Angular distributions of H atoms, with a 5° angle of incidence, reflected from a crystalline Li surface at 300 K for several impact energies. The distributions are shown in the form of a polar diagram with the reflected particle curves normalized to their maximum values. The Lambert cosine law is shown by a dashed line for reference.

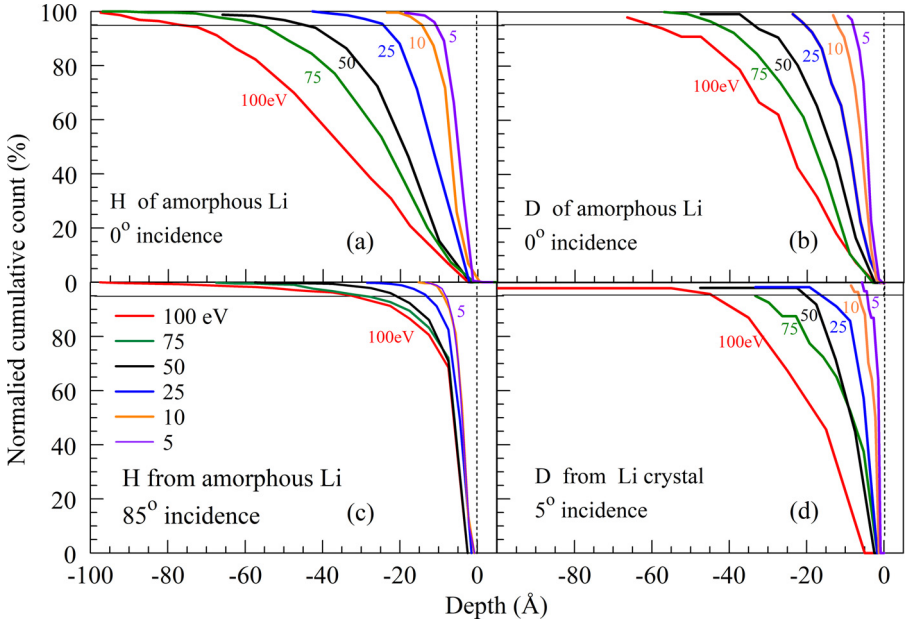

Fig. 10. Reflection depths from amorphous and crystalline Li surfaces for incident H and D atoms at several impact energies. Data is shown for H atoms incident on an amorphous Li surface at (a) 0° and (c) 85° angles of incidence, and for D atoms incident on (b) amorphous and (d) crystalline Li surfaces.

angles θ. This data implies that $E_{a,sp}$ has a weak dependence on the angle of incidence. Indeed, Fig. 15 shows that the energies of sputtered Li atoms, for all angles of H impact at incident energies E in the range of 5-100 eV, have values of 0.1-1.2 eV, with an average value of about 0.5 eV.

The angular distributions of sputtered Li atoms for various angles of incidence of H atoms at an impact energy of 100 eV using Eq. 2 were calculated, as was done for the reflected particles. The angles of the sputtered particles are defined with respect to the surface normal. As seen in Fig. 16, the distributions overall are diffuse, with a tendency toward specular directions when increasing incident angles.

Next, the distribution of the initial positions of the sputtered Li atoms in an amorphous Li slab target was calculated, which is denoted as the "initial sputtering depth". Fig. 17a shows an example of a distribution of initial sputtering depths of sputtered Li atoms with respect to the Li-vacuum interface defined to be 0-depth, resulting from incident H impact at an 85° angle of incidence for var-

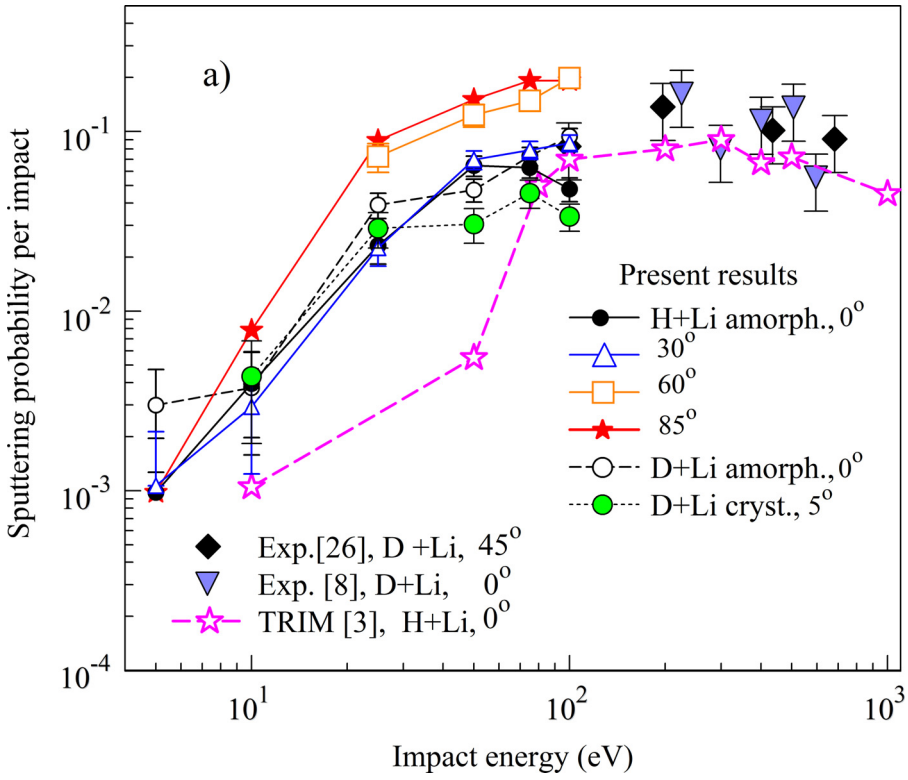

Fig. 11. Sputtering yield of Li atoms per impact of H and D at various angles of incidence in the range of 5-100 eV impact energies for an amorphous and crystalline Li surface at 300 K. Each point is an average over 1000 trajectories. Error bars shown are for maximal standard errors. Comparisons are made to available experimental and TRIM calculation data.

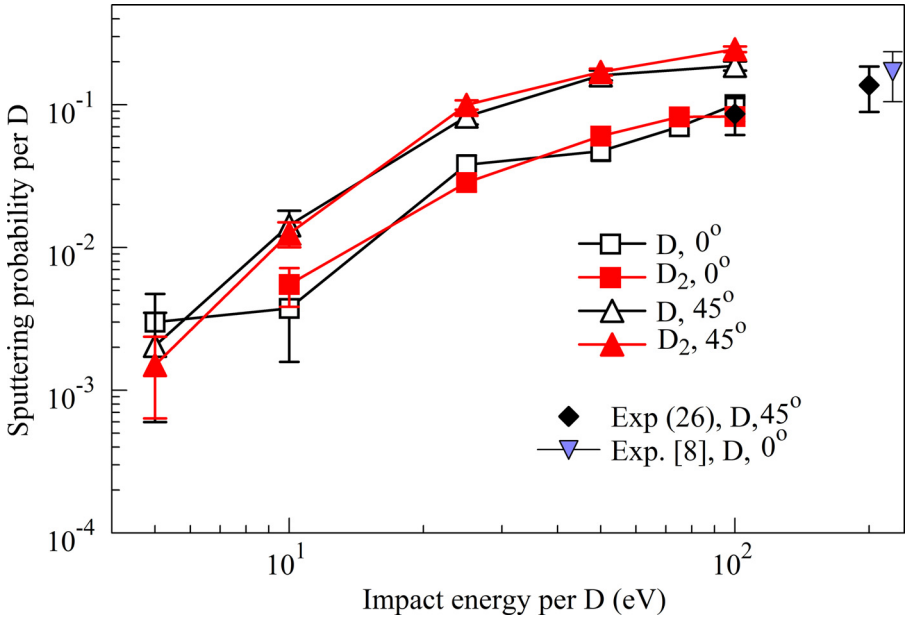

Fig. 12. Sputtering probabilities per D atom for impact of D and D_2 in the range of 5-100 eV impact energies at 0° and 45° angles of incidence at an amorphous Li surface at 300 K. Experimental data for incident D atoms are shown for comparison.

ious impact energies. While the peaks of the distributions stay below 5 Å for all impact energies, their widths increase with increasing impact energy E and the tails extend over 10 Å for $E = 100$ eV. One can calculate the mean initial sputtering depth $\bar{d}$ of each distribution from

$$\bar{d} = \frac{\sum d_i C_i}{\sum C_i} \quad (3)$$

where C_i are counts of the sputtered particles along a distribution in an interval (2 Å taken here) around the sputtering depth d_i. The mean initial sputtering depths as a function of impact energy are shown in Fig. 17b for incident angles of 0°, 30°, and 85° for H, and of 0° for D, from an amorphous Li slab at 300 K. The mean initial sputtering depth increases with impact energy, reaching almost 7 Å for H impact at 100 eV and 0° incidence angle, but is below 4 Å at 25 eV. At 85° angle of incidence, the mean initial sputtering

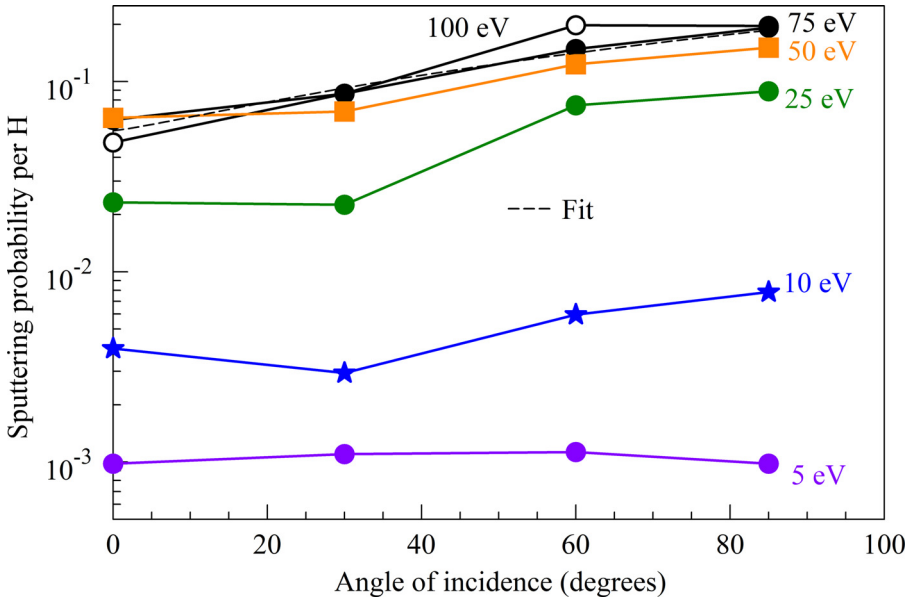

Fig. 13. Sputtering probabilities per H atom for incident H atoms with several impact energies as a function of angle of incidence at an amorphous Li surface at 300 K. The fitted dashed line is explained in the text.

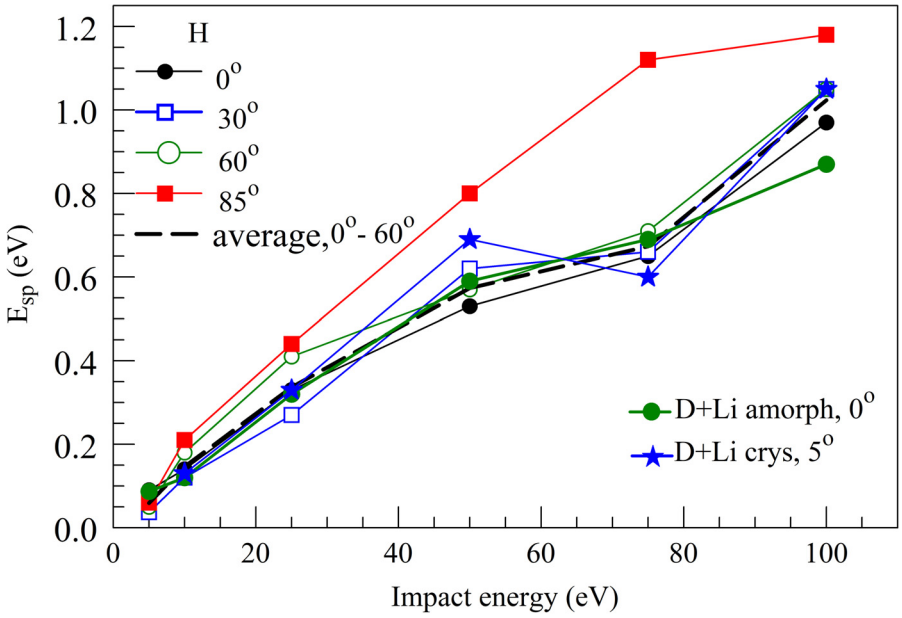

Fig. 14. Average kinetic energies (E_{sp}) of the Li atoms sputtered from the amorphous Li surface as functions of the impact energy E of incident H atoms at various angles of incidence. Averaging is done for each E and θ over all sputtering trajectories. The dashed curve is from data averaged over H incident angles in range of 0-60°. Additional E_{sp} data are also shown for incident D atoms on amorphous and crystalline Li surfaces.

depth stays below 4 Å over the whole considered energy range. These conclusions hold also for a crystalline Li target (not shown here).

One can investigate the mechanism of Li sputtering by incident H atoms by following the trajectories of the incident H atoms that result in Li sputtering. The typical cases are shown in Fig. 18 for two incident angles, 30° and 85°, and for two incident energies, 50 eV and 100 eV. Data points for the curves follow atom positions in the H trajectories, while the arrows show the impact direction of H and the initial direction of the sputtered Li atom. In these considered cases, the sputtering occurs by H atom penetration into the Li slab, reflection off Li atoms that are deep inside the slab, and then on the way toward the surface the H breaks the bond of a Li atom and transfers enough kinetic energy to the Li atom to sputter it into the vacuum. The H atom will either have enough energy to eventually leave the surface also (Fig. 18b) or lose its energy in collisions with Li and be retained in the surface (Fig. 18a). These mechanism types for Li sputtering were observed for most of the H trajectories that resulted in sputtering events, indicating a correlation of the processes of reflection and sputtering for the range of low impact energies considered in this work.

3.3. Retention

As discussed in Section 3.1, the probability of retention is complementary to that of reflection, i.e., $P_{ret} = 1\text{-}P_R$. Therefore, it is not necessary to separately discuss probabilities of retention for various cases of impact particles (H, D, D_2), various impact energies

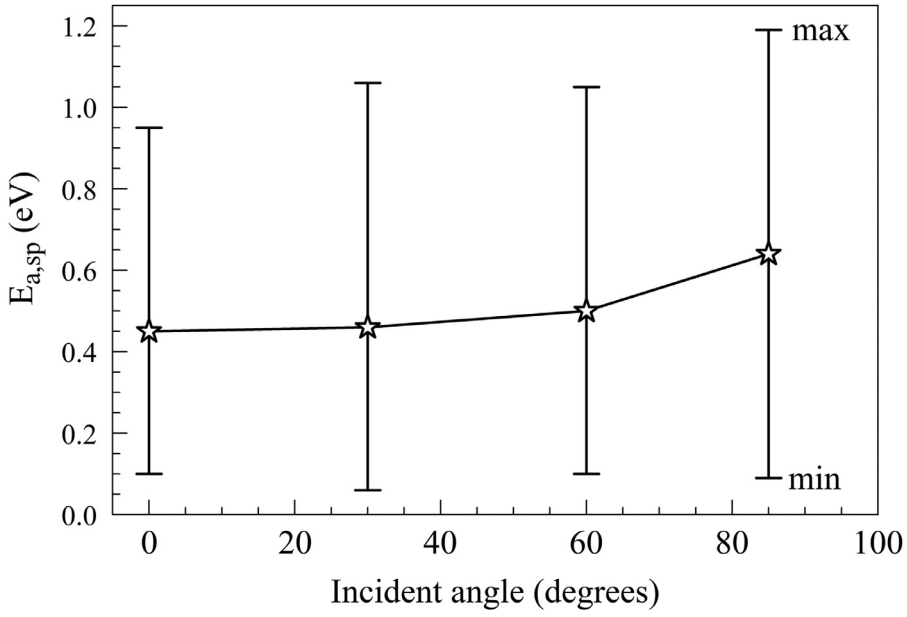

Fig. 15. Average kinetic energies of the sputtered particles, averaged over impact energies of 5-100 eV ($E_{a,sp}$), are plotted for each angle of incidence. The min-max margins reflect the full range of the sputtered energy values for each angle of incidence. The fitted curve is explained in the text.

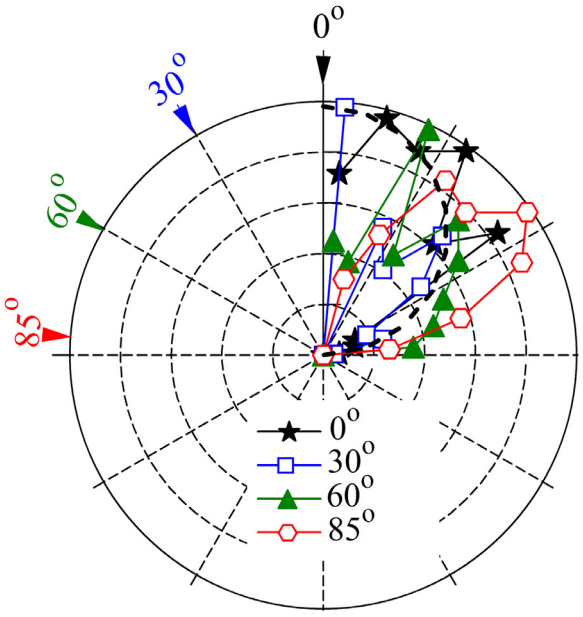

Fig. 16. Angular distributions of Li particles sputtered from an amorphous Li surface at 300 K by H atoms with an impact energy of 100 eV, at several angles of incidence. The distributions are shown in the form of a polar diagram, with reflected particle curves normalized with their maximum values. The Lambert cosine law is shown by a dashed line for reference.

(5-100 eV), various angles of incidence (0-85°) and various target surfaces (amorphous or crystalline). This information is implied in Section 3.1.

The distribution of the retained impact particles inside the slab, at the time scales of the MD calculations, is of interest for estimating the necessary depth of the Li surface slab to properly conduct the calculations. The maximum reflection depth limits, as discussed for Fig. 10, do not exceed 10 nm, indicating that a 10-nm thick Li slab, used in most of this work, is sufficient for studying the reflection and sputtering from a Li surface under the considered conditions. Indeed, when the calculation was done with a 30-nm thick amorphous slab (~100,000 atoms) reflection and sputtering probabilities show only very small differences from the results obtained by using the 10-nm thick slab. However, the retained particles may penetrate deeper than 10 nm with irradiation by energetic atoms, and this is of interest when using thin Li films. If the penetration of the impacting atoms in an experiment is larger than the film thickness, the impacting atoms may interact with the substrate and result in additional reflections and sputtering that are not described by these processes in bulk Li. For this reason, the distributions of the retained particles (Fig. 19) were studied in the described enlarged-depth Li slab using perpendicular incidence of H atoms at 70 eV and 100 eV impact energies and D atoms with 100 eV impact energy. While all cases show a maximum in the distributions at about 5-nm depth, their widths and heights differ significantly. This is best visualized by using the normalized cumulative counts of retained atoms, showing that 90% of impacting H atoms at 100 eV are retained at depths less than about 15 nm, 90% of impacting D atoms at 100 eV are retained at depths less than 12.5 nm, and 90% of impacting H atoms at 70 eV are retained at depths less than 9 nm. The tail of the distribution extends up to 22 nm for retained H atoms incident at 100 eV, up to 20 nm for retained D incident at 100 eV and up to 15 nm for retained H incident at 70 eV. These relatively large depths reached by the retained atoms in Li are certainly a consequence of the low mass density of Li, approximately 0.5 g/cm^3.

3.4. Temperature effects

Molecular dynamics is not convenient for consistent simulation of the phase changes of matter since the time available for MD simulations (typically ns range) is too short to consider diffusion and melting effectively for the nano-size slabs. One way to mitigate this problem and estimate processes of reflection and sputtering at a liquid Li surface by MD is to use a solid amorphized surface slab, as used in Sections 3.1-3.3, and heat it by a Langevin thermostat to temperatures of 500 K and 600 K (above the bulk Li melting point of 453 K at 1 atm pressure). The results using these slabs should partially mimic the processes at the amorphous liquid Li surface. For comparison of similar processes to that of the solid, a crystalline Li slab at 300 K and 400 K were used.

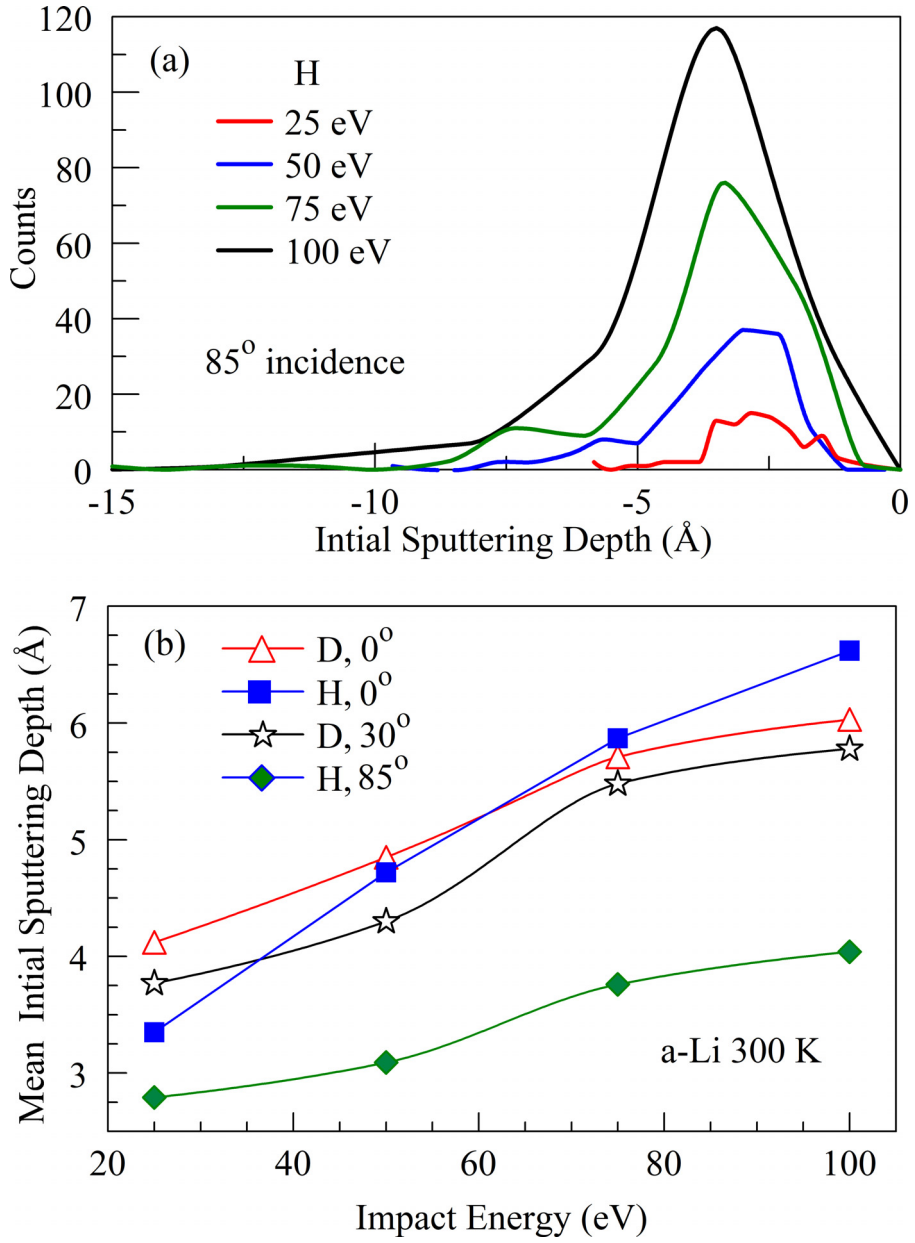

Fig. 17. Initial sputtering depth of Li atoms in an amorphous Li slab target at 300 K, with respect to the surface-vacuum interface (0-depth), due to H and D impacts. (a) Distribution of the initial sputtering depths for several impact energies at an incident angle of 85°. (b) Impact energy dependence of the mean initial sputtering depths, defined by Eq. (3), for various cases of H and D impact.

Fig. 20a shows a plot of the Lindemann index calculated using Eq. 1 for crystalline Li surfaces at 300 K and 400 K and for the amorphous Li surfaces at 500 K and 600 K. The change in the Lindemann parameter over this temperature range shows a characteristic jump across the typical melting point between 400 K and 500 K (thin vertical red line in Fig. 20a is at Li meting temperature of 453 K). For the same samples, calculations of reflection and sputtering probabilities caused by D impacts at 100 eV and 50 eV for 0° incident angles were performed and are presented in Fig. 20b. The reflection and sputtering probability curves increase with increasing temperature, showing the same jump as the Lindemann index in a region between 400 K and 500 K.

The reflection probability for perpendicular D impacts at $E = 100$ eV increases almost three times when the Li temperature increases from 300 K (crystalline) to 600 K ("liquid"), while sputtering increases less than a factor of two over the same temperature range. These changes are somewhat smaller for perpendicular D impacts at $E = 50$ eV. Therefore, the loss of the correlation between Li atoms when transitioning from the solid to liquid phase is reflected in the increase of the Lindeman parameter and the P_R and P_{sp} of D atoms at the Li surface.

4. Discussion and conclusions

Molecular dynamics (MD) calculations were used to study the reflection, retention, and sputtering processes of H and D atoms and D_2 molecules at amorphous and crystalline lithium surfaces at various temperatures. Ranges of particle impact energies (5-100 eV) and angles of incidence (0-85°, where 0° is perpendicular to the surface) were investigated. The MD parameters, such as time steps, preparation of the surface slab, the slab size and temperature, and the number of particle trajectories, were carefully cho-

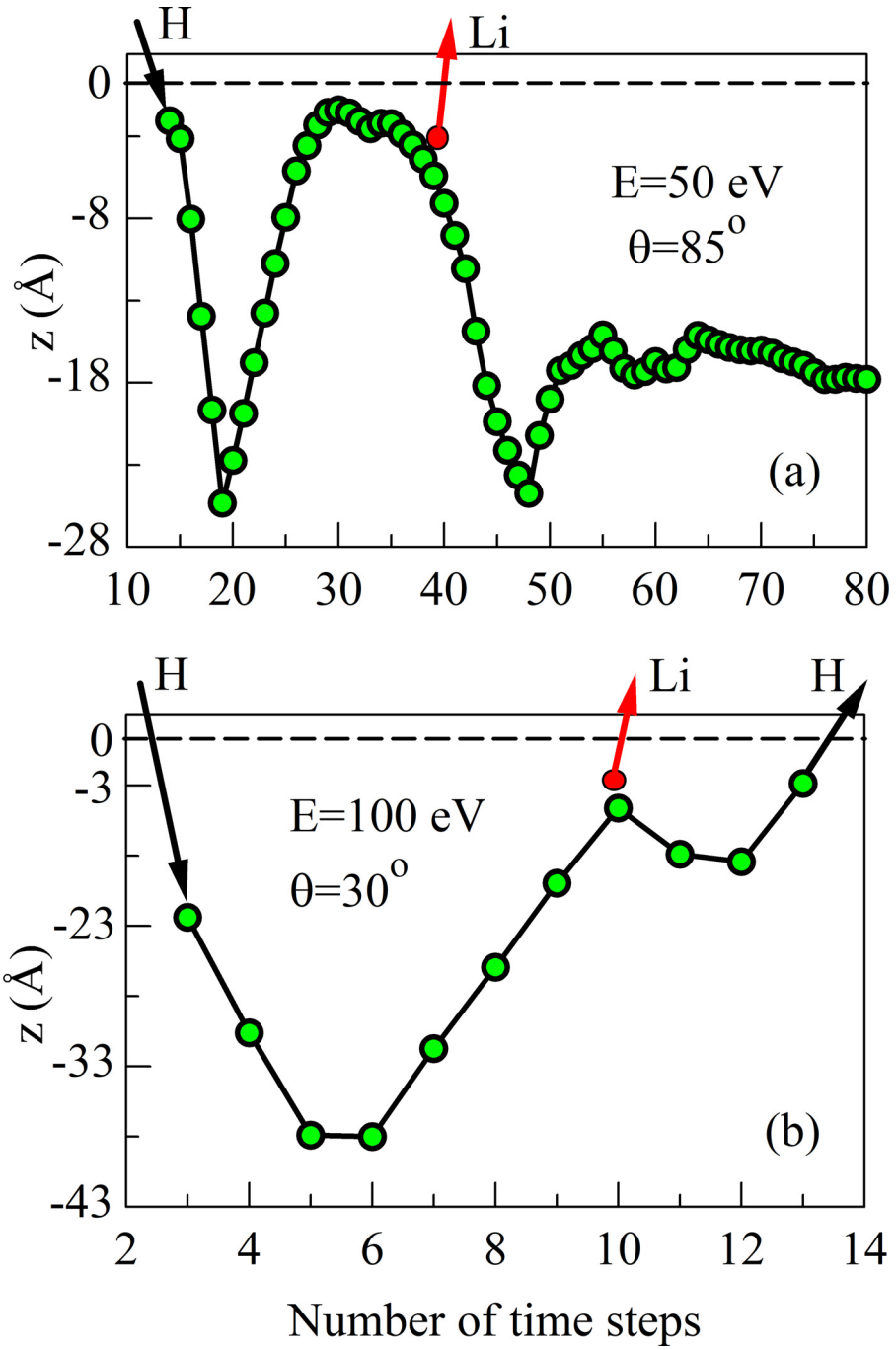

Fig. 18. Mechanisms of Li sputtering upon H irradiation of an amorphous Li surface (85°) at 300 K. Typical cases are shown: In (a) for H atoms at 50 eV impact energy and high incident angle (85°), and (b) for H atoms at 100 eV impact energy at a low incident angle (30°). Vacuum-Li interface is shown by dashed line, and directions of impact, sputtered and reflected particles are schematically presented by arrows.

sen based on relevant computational experiments. Reflection, retention, and sputtering probabilities for any given set of conditions were obtained "on the same footing". The probabilities and their uncertainties were obtained by scanning the surface at different points using independent impacts and were calculated as average values per impact atom and reported with maximal standard error values. Since retention and reflection probabilities must sum together to be unity, we found it sufficient to discuss only the reflection and sputtering results in detail.

The reflection probabilities for incident H and D atoms and D_2 molecules at an amorphous Li surface have a stronger dependence on the angles of incidence of the particles than on the particle impact energy E, for $E < 100$ eV, especially for energies above 25 eV. Reflection of incident D atoms at an amorphous Li surface is significantly lower than that of incident H atoms. On the other hand, D reflection at a crystalline Li surface is smaller than that at an amorphous Li surface over the impact energy range of $10 < E \leq 100$ eV and decreases with increasing energy, which could be attributed to channeling effects. Incident D_2 molecules were mostly not reflected and most impacts dissociated at the surface, with D atoms either retained in or reflected from the surface after dissociation. D_2 reflection probabilities (per D atom) almost coincide with those for D atom impacts, except at the lowest impact energies (5-10 eV) close to the D_2 bond dissociation energy (~4.5 eV).

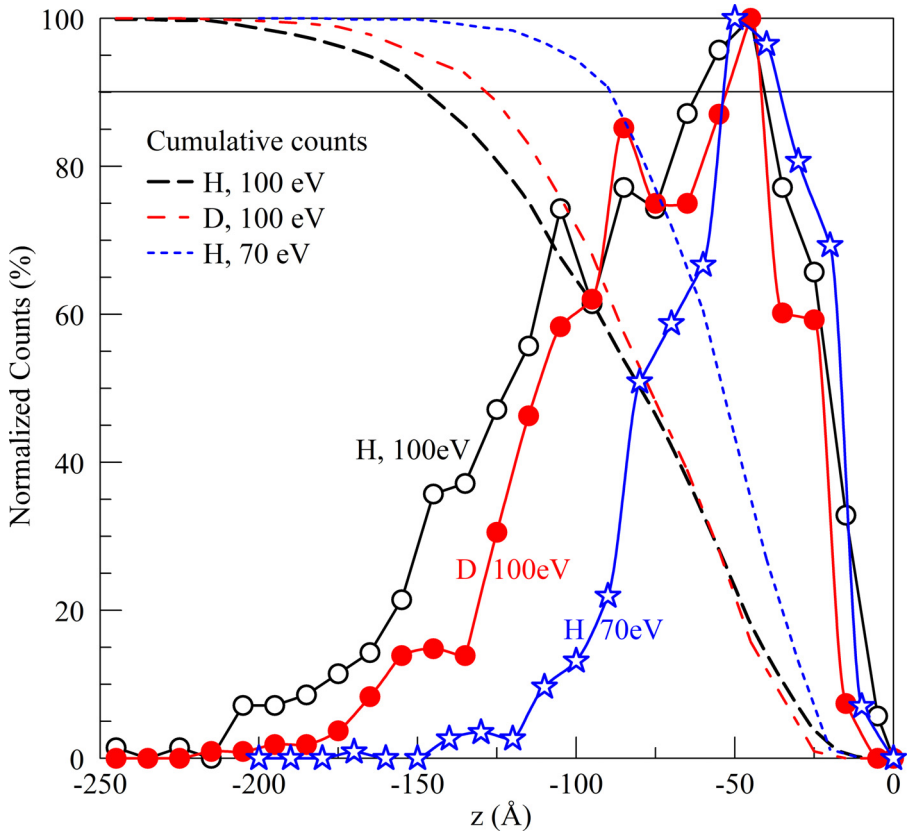

Fig. 19. Distributions of retained atoms in an amorphous Li surface at 300 K (solid lines) and normalized cumulative counts (in %) of the retained atoms (dashed lines). Normalization was done by scaling the maximum cumulative counts for each data set and condition to 100%.

Energy distributions of the ratio of the energy of a reflected atom and its impact energy E are weak functions of E, with a much stronger dependence on the particle incident angle. Thus, this ratio reaches 0.8 for incident angles of 85°, but is below 0.5 for incident angles less than 30°. This is a consequence of significantly deeper penetration before reflection for smaller impact angles, nearer to the surface normal, which increases the possibility that the reflected particle collides with other Li atoms before leaving the surface. The energies of reflected D atoms are smaller than that for H atoms, which is likely a consequence of the higher fraction of energy transferred to Li atoms by impacts with D than with H. The angular distributions of the reflected particles are irregular-diffuse. While the penetration depth of reflected particles is about 8 nm and 1.5 nm for H impacts at 100 eV and 10 eV, respectively, at 0° incidence, it is much smaller at 85° incidence, with penetration depths of 4 nm and 0.5 nm at the same impact energies. The penetration depth is smaller for reflected D than H atoms, 6 nm and 1 nm for D impacts at 100 eV and 10 eV, respectively, and 0° incidence, which is further decreased if the Li surface is crystalline.

Unlike reflection, sputtering probabilities for particle impacts have a weaker dependence on the incident angles than on the impact energies, changing two orders of magnitude over the considered energy range, but only up to a factor of three when changing from 0° to 85° incidence. Sputtering probabilities by H, D, and D_2 deviate from each other only within the values of the maximal standard error. However, the sputtering probabilities for D incident at a crystalline Li surface is persistently smaller than that at an amorphous Li surface for impact energies above 25 eV. The average energy of sputtered Li atoms changes from 0.1 eV to 1 eV when the impact energy changes from 5 eV to 100 eV, irrespective of the type of impact particle (H or D), type of surface (amorphous or crystalline), or angle of incidence. The exception is sputtered Li particles by irradiation with particles at almost a grazing angle of incidence (85°), which persistently have 20-30% larger energy than for the other cases. The angular distributions of the sputtered Li particles are irregular-diffuse, like in the case of reflection. The distributions of the depth of origination of the sputtered Li particles peak below 0.5 nm, though the distribution widths increase with particle impact energy, with tails reaching 1 nm at 100 eV impact energy and 0° incident angle. The average sputtering origination depths for various angles of incidence vary from 0.35 nm to 0.65 nm when the impact energy changes from 5 eV to 100 eV, for both H and D impacts. The exception is the incident angle of 85°, where the average sputtering origination depth varies from 0.275 nm to 0.375 nm. The most common mechanism of sputtering was also discussed, which we observed for most trajectories that lead to sputtering. It was found that a Li atom is kicked out from the surface not directly by an impact particle on its incoming trajectory, but rather when it reflects and, on the way-out "kicks out" a Li atom close to the surface-vacuum interface by breaking Li-Li bonds in the surface. In that process, the incident H or D particle may lose enough energy to stay in the surface, or rarely, may still have enough energy to leave the surface together with the sputtered particle. We name this process at low impact energies *reflective sputtering*.

The penetration depth of the retained atoms shows unique features due to the low mass density of lithium (~0.5 g/cm^3). While the maximum penetration depth of the reflected particles is smaller than 10 nm, retained H atoms can reach a depth of 20 nm (smaller for D) on the timescale of the MD simulations, which decreases with impact energy and incident angle. The information on the penetration of both reflected and retained particles has significance both for the size of the target slab in simulations and for experiments of the effects of another material substrate

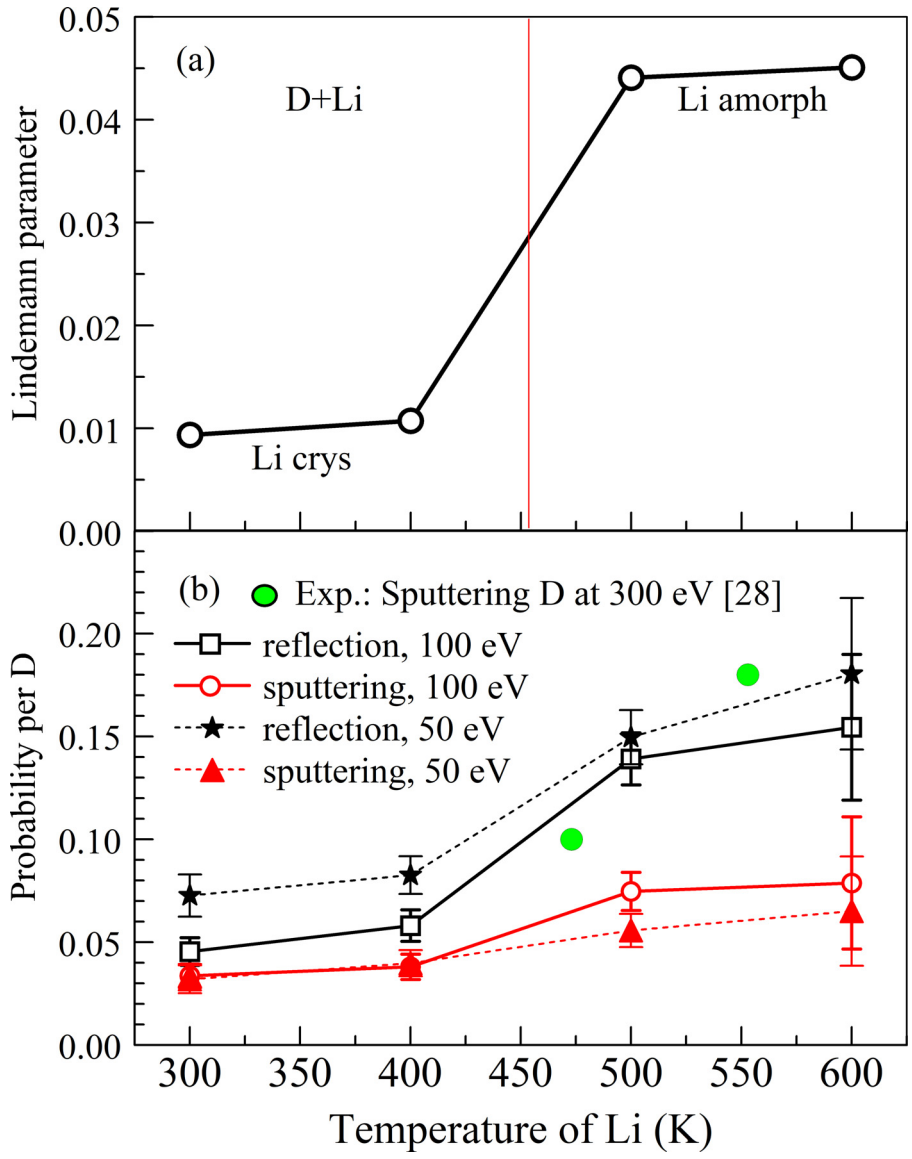

Fig. 20. (a) Lindemann index for the Li surface as a function of temperature. The thin vertical line is the bulk Li melting point of 453 K at 1 atm pressure. (b) Reflection and sputtering probabilities at an amorphous Li surface by perpendicular D impacts as functions of the Li surface temperature. Experimental sputtering data from Ref. [28] is added for comparison.

on the reflection, retention, and sputtering from very thin lithium films.

We have speculated on the effects of lithium surface temperature and its aggregate state (solid vs. liquid). Although solid amorphous structures are typical for PFC surfaces exposed to the high fluxes and fluences of fusion plasma particles, justifying our studies with solid Li surface slabs, it was shown that there is an increase of the reflection (250%) and sputtering (80%) probabilities when a crystalline Li slab at 400 K is heated up to form an amorphous Li slab at 500 K. The transition mimics the step increase of the Lindemann parameter at the Li melting temperature. This result indicates the possibility of comparing surface processes at an amorphous heated Li slab with those at a liquid Li surface. These results still need to be confirmed by ongoing experiments in our group.

Accumulated hydrogen in a Li surface irradiated by a H (or D) beam or plasma will form lithium hydride. Additionally, lithium oxide and lithium hydroxide are often present in lithiated PFCs due to reactions with background vacuum gases such as water. Consequently, further computational, and experimental studies of the surface processes for these compounds are required. These are the subject of our current studies and will be detailed in our future publications.

Declaration of Competing Interest

The authors declare that they have no known competing financial interests or personal relationships that could have appeared to influence the work reported in this paper.

CRediT authorship contribution statement

P.S. Krstic: Conceptualization, Methodology, Software, Validation, Data curation, Formal analysis, Investigation, Resources, Writing – original draft, Visualization. **E.T. Ostrowski:** Writing – review & editing, Visualization, Validation. **F.J. Domínguez-Gutierrez:** Writing – review & editing, Visualization, Data curation, Software. **S. Abe:** Writing – review & editing, Visualization. **B.E. Koel:** Supervision, Writing – review & editing, Project administration, Funding acquisition, Resources, Validation.

Acknowledgments

This material is based upon work by the U.S. Department of Energy, Office of Science/Fusion Energy Sciences under Award Number DE-SC0019308. PK is grateful to Princeton University for using the Stellar HPC cluster, to Stony Brook University for access to the SeaWulf HPC, and to XSEDE for access to the SDSC Expanse and Comet HPC through grant TG-DMR110037 and allocation UTK101. PK is grateful to Adri van Duin of PSU for improvement of the Li-H ReaxFF.

References

[1] R. Majeski, R Doerner, T. Gray, et al., Phys. Rev. Lett. 97 (2006) 4.
[2] M.G. Bell, H.W. Kugel, R. Kaita, et al., Plasma Phys. Control. Fus. 51 (2009) 124056.
[3] R. Majeski, R.E. Bell, D.P. Boyle, et al., Phys. Plasma 23 (2017) 13.
[4] D.P. Boyle, R. Majeski, J.C. Schmitt, et al., Phys. Rev. Lett. 119 (2006) 015001.
[5] M. Lucia, R. Kaita, R. Majeski, et al., J. Nucl. Mater 463 (2015) 907.
[6] J.P. Allain, D.N. Ruzic, M.R. Hendricks, et al., J. Nucl. Mater. 290 (2001) 180.
[7] J.P. Allain, J.N. Brooks, D.A. Alman e t al, J. Nucl. Mater. 337 (2005) 94.
[8] C.H. Skinner, R. Sullenberger, B.E. Koel, et al., J. Nucl. Mater. 438 (2013) 136.
[9] L. Buzi, A.O. Nelson, Y. Yang, et al., J. Nucl. Mater. 19 (2019) 411.
[10] L. Pauling, J. Am. Chem. Soc. 54 (1932) 3570.
[11] L.C. Allen, J. Am. Chem. Soc. 111 (1989) 9003.
[12] P.S. Krstic, J.P. Allain, A. Allouche, et al., Fusion Eng. Design 87 (2012) 1732.
[13] P.S. Krstic, et al., Phys. Rev. Lett. 110 (2013) 105001.
[14] P.S. Krstić, R.J. Harrison, B.G. Sumpter, Phys. Scr. T124 (2006) 101.
[15] Adri C.T.van Duin, S. Dasgupta, F. Lorant, et al., J. Phys. Chem. A 105 (2001) 9396.
[16] S.S. Han, Adri C.T.van Duin, W.A. Goddard III, et al., J. Phys. Chem. A 109 (2005) 4575.
[17] F.J. Domínguez-Gutiérrez, P.S. Krstic, J.P. Allain, F. Bedoya, M. Islam, R. Lotfi, A.C.T. van Duin, J. Appl. Phys. 123 (2018) 195901.
[18] A. Lele, P. Krstic, A.C.T. van Duin, J. Chem. Phys. A 126 (2022) 568.
[19] M. Elstner, et al., Phys. Rev. B 58 (1998) 7260.
[20] S. Plimpton, J. Comput. Phys. 117 (1995) 1.
[21] L. Buzi, Y. Yang, F.J. Dominguez-Gutierrez, et al., J. Nucl. Mater. 502 (2018) 161.
[22] F.J. Dominguez-Gutierrez, F. Bedoya, P.S. Krstic, et al., Nucl. Fusion 57 (2017) 086050 and references therein.
[23] F.J. Dominguez-Gutierrez, P.S. Krstic, J. Nucl. Mater. 492 (2017) 56.
[24] P.S. Krstic, C.O. Reinhold, S.J. Stuart, Europhys. Lett. 77 (2007) 33002.
[25] P.S. Krstic, Han L, S. Irle, H. Nakai, Chem. Sci. 9 (2018) 3803 and references therein.
[26] J.P. Allain, D.N. Ruzic, Nucl. Fusion 42 (2002) 202.
[27] Hua-Tan Qiu, D.N. Ruzic, J. Nucl. Mater. 337-339 (2005) 1029.
[28] J.P. Allain, M.D. Coventry, D.N. Ruzic, Phys. Rev. B 76 (2007) 205434.
[29] P.S. Krstic, C.O. Reinhold, S.J. Stuart, J. Appl. Phys. 104 (2008) 103308.
[30] F.J. Domínguez-Gutiérrez, P.S. Krstic, J. Appl. Phys. 121 (2017) 215302.
[31] J.A. Dean, Lange's Handbook of Chemistry, 15 edition, Mc Graw-Hill, 1999.